Structural analysis of adhesive joints using meshless methods

Luís D.C. Ramalho[1], Isidro J. Sánchez-Arce[2], Diogo C. Gonçalves[1], Raul D.S.G. Campilho[1,3], Jorge Belinha[1,3]

[1]*INEGI, Institute of Mechanical Engineering*
Rua Dr. Roberto Frias, 4200-465, Porto, Portugal
lramalho@inegi.up.pt, costa.goncalves.diogo@gmail.com
[2]*UTAD, University of Trás-os-Montes and Alto Douro*
Quinta de Prados, 5000-801, Vila Real, Portugal
isidrodjsa@gmail.com
[3]*ISEP-School of Engineering, Polytechnic of Porto*
Rua Dr. António Bernardino de Almeida, 431, 4200-072, Porto, Portugal
raulcampilho@gmail.com, job@isep.ipp.pt

Abstract. Adhesive bonding is a joining method that presents several advantages in comparison to other commonly used techniques, such as bolting or riveting. One notable advantage is the relative lightweight nature of adhesive joints, which holds significant relevance in the pursuit of more efficient transportation vehicles. It is well-known that lighter vehicles consume less energy, making this a desirable characteristic. Given the growing interest in adhesive joints, it becomes crucial to thoroughly investigate their behaviour under various conditions. Currently, the literature contains several documents describing the structural behaviour of adhesive joints, with numerous research numerical studies using as numerical discretization method the finite element method (FEM). However, other mature advanced discretization techniques are also available to the computational mechanic's research community, such as meshless methods. This work proposes to show several numerical applications of adhesive joints using meshless methods. Static and dynamic demanding examples are addressed, and the results are compared with solutions obtained with the FEM. The results show the efficiency of meshless methods, proving that such discretization techniques are valid alternatives to the FEM. Additionally, this work provides valuable insights and knowledge that are currently lacking, ultimately enhancing our understanding of adhesive joints and their behaviour under static and varying dynamic conditions.

Keywords: Adhesive joints, Radial point interpolation method, Natural neighbours radial point interpolation method, continuum mechanics criterion

1 Introduction

Adhesive joints are used in a wide range of products, such as cars, airplanes, wind turbines, etc. This makes it important to have sophisticated analysis methods to assess, among other things, the strength of adhesive joints. Numerical simulations are advantageous in this because they are generally cheaper than experimental tests. The strength of adhesive joints has been traditionally predicted using the conventional Finite Element Method (FEM). However, the oldest models are analytical models, like the Volkernsen model [1], these models are generally more limited in scope than numerical methods like the FEM, hence they are used less frequently nowadays. De Sousa et al. [2] provide a good comparison of many different analytical methods.

Other alternatives to the FEM are the eXtended FEM (XFEM) and meshless methods. The XFEM uses enriched displacement functions to simulate crack propagation, it has been used in adhesive joints with some success, like in the work of Silva et al. [3]. Meshless methods are a group of advanced numerical methods, there are many types of meshless methods that differ from each other in the shape functions, in the formulation or in the integration [4]. In this work two different meshless methods are used. The first method is the Radial Point Interpolation Method (RPIM), this method was proposed by Wang and Liu [5]. The second meshless method used in this work is the Natural Neighbours RPIM (NNRPIM) [6], this method is similar to the RPIM in many

aspects, but it has a different way of creating the integration points and their respective influence domains, which are equivalent to elements in the FEM. Both the RPIM and the NNRPIM have already some works published in the field of adhesive joints [7, 8], but nothing comparable to the amount of works using the FEM.

Regardless of the numerical method the strength of adhesive joints is usually predicted using continuum, fracture or damage criteria, or Cohesive Zone Models (CZM). The review by Ramalho et al. [9] shows that CZM are the most popular method of predicting the strength of adhesive joint under static loads. CZM use cohesive elements that describe the relationship between the connected nodes using a traction-separation law. The main problem with CZM is that some properties of the traction-separation law change with adhesive thickness [10]. Even so, CZM are extensively used because they provide strength predictions with minimal errors, they have been used to predict the strength of several types of joints, including Single Lap Joints (SLJ) [11]. Continuum mechanics criteria predict the strength of adhesive joints using just the stress or strain. This type of criterion has a limitation, which is the stress singularity created at the adhesive-adherent interface corner. This singularity means that the stresses and strains in that region are discretization-dependent [12]. An alternative to this is using the stress in the middle of the adhesive layer to predict the strength, this avoids the stress singularity, but it usually results in strength under-predictions, since failure generally starts near the adhesive-adherent interface corner. The Critical Longitudinal Strain (CLS) criterion [13] is a recent continuum mechanics criterion that seems to provide accurate strength predictions for SLJ. Therefore, this was the criterion chosen for this work. Fracture mechanics criterion make use of the stress intensity factor, or similar fracture mechanics concepts, to predict the strength of adhesive joints. One example of this it the Intensity of Singular Stress Fields (ISSF) criterion used by Dionísio et al. [14]. Lastly, damage mechanics criteria are criteria where the mechanical properties of the adhesive, or adherents, are degraded, due to the loads, until failure, and strength is predicted in that way like in the work of Zhang et al. [15].

Considering the limited amount of works dedicated to meshless methods in adhesive joints, this work aims at comparing the RPIM and the NNRPIM to the FEM in the strength prediction of a SLJ, using the CLS criterion.

2 Numerical Model

In this work two different meshless methods were used, namely: the RPIM and the NNRPIM. These two methods have many similarities, but they differ in the way the integration points are created and how their respective influence domains are determined. Both numerical methods start by discretizing a given domain Ω into a nodal set $\mathbf{N}$. After this the two numerical methods diverge in the creation of integration points and in the way their influence domains are determine. This process is described in detail in Section 2.1 for the RPIM and in Section 2.2 for the NNRPIM.

Having the integration points and respective influence domains determined, it is then possible to calculate the shape functions, this process is the same for both numerical methods, and it is described in 2.3. These shape functions are composed by a polynomial function and a RBF. The rest of the implementation of both the RPIM and the NNRPIM is very similar to the FEM and can be found in references [4, 16].

2.1 Radial Point Interpolation Method

In the RPIM a background integration grid is used to aid in the creation of the integration points. In this work the grid is composed of quadrilaterals and the integration points are created inside them using a 2×2 Gauss-Legendre quadrature, this is exemplified in fig. 1a. Then, the influence domain of each integration point is determined. There are several ways to do this, described by Belinha [4]. In this work the influence domains are composed by the 16 nodes closest to the integration points, just like in the two example influence domains in fig. 1a. This influence domain size is within the recommended range found in literature [4]. In fig. 1a the two influence domains share some nodes, this is called domain overlapping, and it is what ensures domain connectivity in the RPIM. Every node will belong to the influence domain of several integration points [4].

In adhesive joints there are material interfaces, this can be troublesome for the influence domains in the RPIM. This is exemplified in fig. 2a, where the influence domains of integration points of a given material are composed by nodes inside the other material. This problem is more significant in adhesive joints since the discretization of the adhesive layer is significantly finer than the adherent discretization. To solve this problem the solution exemplified in fig. 2b was adopted. This solution consists in limiting the influence domains of integration points in a given material to nodes also of that material and nodes in the interface region. This solution is similar to the solution adopted by Cordes and Moran [17] for the Element Free Galerkin (EFG) method.

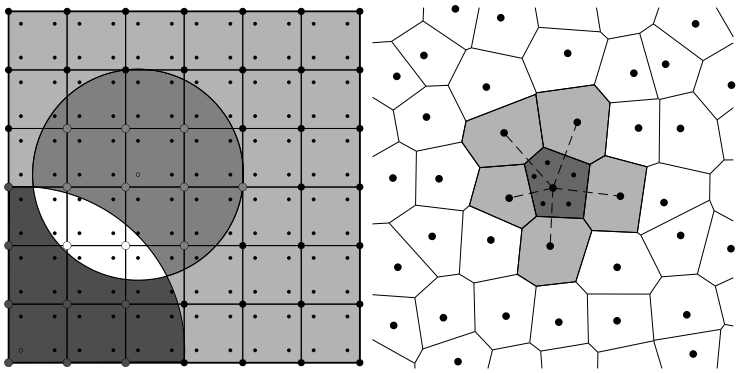

(a) (b)

Figure 1. Creation of integration points and influence domains in (a) the RPIM and (b) the NNRPIM with an irregular nodal distribution

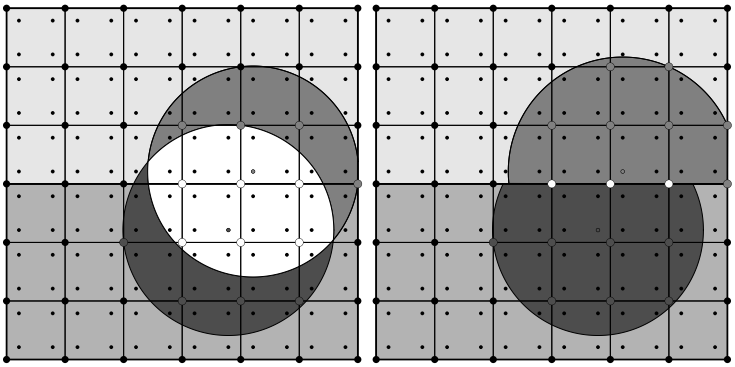

(a) (b)

Figure 2. (a) No restriction, (b) and restriction of the influence domains at a material interface

2.2 Natural Neighbours Radial Point Interpolation Method

The NNRPIM uses another approach, instead of having influence domains it has influence cells, and the integration points are created using Voronoi cells and the Delaunay triangulation. In this work, the integration points are created at the centre of each subdivision made by the Voronoi cells and the Delaunay triangulation, just like in fig. 1b, where the dashed lines are the Delaunay triangulation and the lines are the Voronoi diagrams. Then, the influence cell of each integration point will be composed by its natural neighbours, which are the node of its own Voronoi cell and the nodes of neighbouring Voronoi cells, as shown in fig. 1b. This means that the integration points shown in fig. 1b will have all the nodes inside the grey Voronoi cells in their influence cells.

2.3 Shape Functions

The shape function of the RPIM and the NNRPIM are calculated in the same manner, they combine polynomial and a Radial Basis Function (RBF). Pascal's triangle is used to define the polynomial function. In this work, a linear polynomial is used for the RPIM, so $\mathbf{p}(\mathbf{x}_i) = [1\ x_i\ y_i]$, and a constant polynomial is used for the NNRPIM $\mathbf{p}(\mathbf{x}_i) = [1]$, , being x_i and y_i the coordinates of point i. Regarding the RBF several different alternatives can be used, one commonly used RBF is the Multi-Quadrics RBF (MQ-RBF), which is the one adopted in this work. This RBF is defined as $r_i(x_j) = (d_{ij}^2 + (\gamma \cdot d_a)^2)^p$, being γ and p function shape parameters, d_a the weight of the integration point, and d_{ij} the Euclidean norm between points i and j. The ideal shape parameter values have been previously studied by Liu and Wang [18] for the RPIM and by Belinha [4] for the NNRPIM. In those works the ideal parameters for the RPIM were found to be $p = 1.03$ and $\gamma = 1.42$, and $p = 0.9999$ and $\gamma = 1.0001$ for the NNRPIM. Having both the polynomial and the RBF, the RPIM shape functions are determined with the following calculation:

$$\left\{\boldsymbol{\Phi}(\mathbf{x}_I)^T \qquad \boldsymbol{\Psi}(\mathbf{x}_I)^T\right\} = \left\{\mathbf{r}(\mathbf{x}_I)^T \qquad \mathbf{p}(\mathbf{x}_I)^T\right\} {\mathbf{M_T}}^{-1} \tag{1}$$

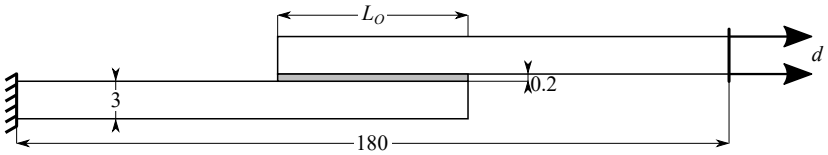

Figure 3. Joint dimensions

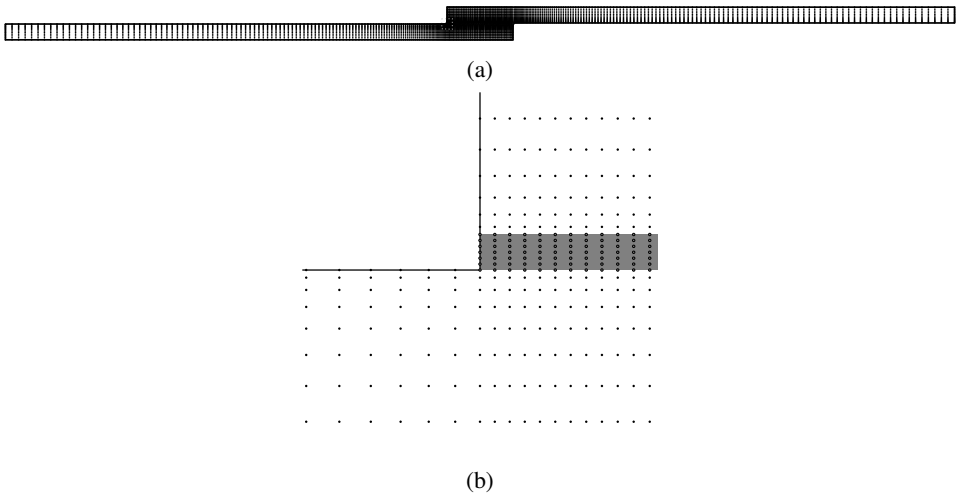

Figure 4. (a) Discretization of the $L_{\mathrm{O}} = 12.5$ mm joint, (b) and detail near the adhesive/adherent corner

where $\mathbf{r}(\mathbf{x}_I)$ is the and column vector of the RBF, and $\mathbf{p}(\mathbf{x}_I)$ is the column vector of the polynomial for the integration point $\mathbf{x}_I$, and:

$$\mathbf{M_T}^{-1} = \begin{bmatrix} \mathbf{R} & \mathbf{R} \\ \mathbf{P}^T & \mathbf{Z} \end{bmatrix} \tag{2}$$

being $\mathbf{R}$ and $\mathbf{P}$ matrices built with the RBF and polynomial function values at each node. In eq. 1, $\mathbf{\Phi}(\mathbf{x}_I)$ is the vector containing the shape functions of integration point $\mathbf{x}_I$ and $\mathbf{\Psi}(\mathbf{x}_I)$ is a by-product vector with no relevant meaning. The full development leading to these shape functions is presented in reference [4].

3 Numerical Results

3.1 Model and Discretization

The analysis presented in this section is relative to a SLJ, presented in fig. 3, subjected to an imposed displacement. All joint dimensions are fixed, except the overlap length (L_{O}), where four different L_{O} were tested: 12.5 mm, 25 mm, 37.5 mm and 50 mm. For the CLS criterion at least two different L_{O} are needed to determine the critical parameters. This joint is composed of two different materials, the substrate and the adhesive. In this the substrates are aluminium and three different adhesives were tested. The aluminium substrates have the following mechanical properties: $E = 70.07 \pm 0.83$ GPa, $\nu = 0.3$. The three different have the following properties: Araldite® AV138 has 4.89 ± 0.81 GPa and $\nu = 0.35$, Araldite® 2015 has $E = 1.85 \pm 0.21$ GPa and $\nu = 0.33$, and Sikaforce® 7888 has $E = 1.89 \pm 0.81$ GPa and $\nu = 0.33$ [2].

The discretizations for all L_{O} are similar to the discretization for the $L_{\mathrm{O}} = 12.5$ mm case shown in fig. 3. These discretization always have 7 lines of nodes along the adhesive thickness, and a bias effect along the adhesive length, and the adherent length and thickness. This bias ensures that there is a higher nodal concentration near the overlap ends, which is the region with a higher stress concentration. All simulations were made assuming linear-elastic, linear-geometric and plane-strain behaviour.

Table 1. CLS parameters for the Araldite® AV138

		FEM		RPIM		NNRPIM	
L_{O1} (mm)	L_{O2} (mm)	r_c	ε_c	r_c	ε_c	r_c	ε_c
12.5	25	0.0455	2.08×10^{-3}	0.0420	2.06×10^{-3}	0.0477	2.08×10^{-3}
	37.5	0.0409	2.04×10^{-3}	0.0375	1.97×10^{-3}	0.0429	2.02×10^{-3}
	50	0.0372	1.92×10^{-3}	0.0334	1.85×10^{-3}	0.0387	1.91×10^{-3}
25	37.5	0.0271	2.34×10^{-3}	0.0245	2.34×10^{-3}	0.0273	2.36×10^{-3}
	50	0.0220	2.31×10^{-3}	0.0201	2.29×10^{-3}	0.0227	2.32×10^{-3}
37.5	50	0.0152	2.52×10^{-3}	0.0145	2.52×10^{-3}	0.0162	2.53×10^{-3}

Table 2. CLS parameters for the Araldite® 2015

		FEM		RPIM		NNRPIM	
L_{O1} (mm)	L_{O2} (mm)	r_c	ε_c	r_c	ε_c	r_c	ε_c
12.5	25	0.1413	1.48×10^{-3}	0.1222	1.45×10^{-3}	0.1384	1.51×10^{-3}
	37.5	0.1056	1.67×10^{-3}	0.0895	1.69×10^{-3}	0.1027	1.71×10^{-3}
	50	0.0778	1.85×10^{-3}	0.0645	1.89×10^{-3}	0.0761	1.89×10^{-3}
25	37.5	0.0630	2.40×10^{-3}	0.0429	2.65×10^{-3}	0.0594	2.50×10^{-3}
	50	0.0365	2.88×10^{-3}	0.0276	3.00×10^{-3}	0.0350	2.97×10^{-3}
37.5	50	0.0175	3.66×10^{-3}	0.0164	3.64×10^{-3}	0.0187	3.65×10^{-3}

3.2 Critical Longitudinal Strain

The CLS criterion is a criterion based on the theory of critical distances [19] and it was first proposed by Ayatollahi and Akhavan-Safar [13]. It is used to predict the strength of only SLJ by defining that it fails when a critical longitudinal strain (ε_c) is reached at a critical distance (r_c). These two critical parameters are determined by a combination of experimental tests and numerical simulations to SLJ with two different L_{O}. The experimental results are obtained from [8]. The process to determine the critical parameters is the following: initially, the experimental tests of SLJ with different L_{O} are conducted and their experimental strength is determined; afterwards, this force determined in the experiments is applied to the SLJ in a linear-elastic numerical simulation under the same conditions of the experimental tests; then, a plot of the longitudinal strains (ε_{xx}) along the adhesive mid-thickness plane for both L_{O}, with the distance normalized; the final step is to determine the intersection between the ε_{xx} curves of both L_{O}, this point gives the ε_c and r_c parameters.

Following this procedure, the critical strains and points were determined for the various adhesives, with the two meshless methods and the FEM, which serves as a comparison. The influence of the L_{O} was also assessed by determining the critical parameters with every possible L_{O} combination. The CLS parameters for the different adhesives are shown in Table 1, Table 2 and Table 3. The critical parameters determined with the FEM and the NNRPIM are similar, but the RPIM is slightly different from the other two numerical methods, with the r_c being lower, which in turn will influence the ε_{xx}. The parameters also tend to vary with the L_{O} combination chosen, regardless of the numerical method and adhesive used.

3.3 CLS Strength Prediction

Using the critical parameter values from Table 1, Table 2 and Table 3 the strength predictions were performed for the joint using the three different numerical methods. Since the critical parameters change depending on the L_{O} combination used. When considering the absolute error, the strength predictions were most accurate with the $L_{O1} = 12.5$ mm and $L_{O2} = 37.5$ mm combination, for all adhesives and numerical methods. With that L_{O} combination the highest error was 14.27%, 15.08%, and 14.87%, with the FEM, the RPIM and the NNRPIM, respectively. This occurred when predicting the strength of the joint with Araldite® 2015 and $L_{\mathrm{O}} = 50$ mm. On

Table 3. CLS parameters for the Sikaforce® 7888

		FEM		RPIM		NNRPIM	
L_{O1} (mm)	L_{O2} (mm)	r_c	ε_c	r_c	ε_c	r_c	ε_c
12.5	25	0.1358	2.21×10^{-3}	0.1160	2.19×10^{-3}	0.1330	2.26×10^{-3}
	37.5	0.1011	2.49×10^{-3}	0.0842	2.54×10^{-3}	0.0984	2.55×10^{-3}
	50	0.0921	2.57×10^{-3}	0.0790	2.60×10^{-3}	0.0894	2.64×10^{-3}
25	37.5	0.0609	3.52×10^{-3}	0.0411	3.90×10^{-3}	0.0570	3.67×10^{-3}
	50	0.0591	3.56×10^{-3}	0.0478	3.63×10^{-3}	0.0572	3.66×10^{-3}
37.5	50	0.0571	3.64×10^{-3}	0.0496	3.55×10^{-3}	0.0574	3.65×10^{-3}

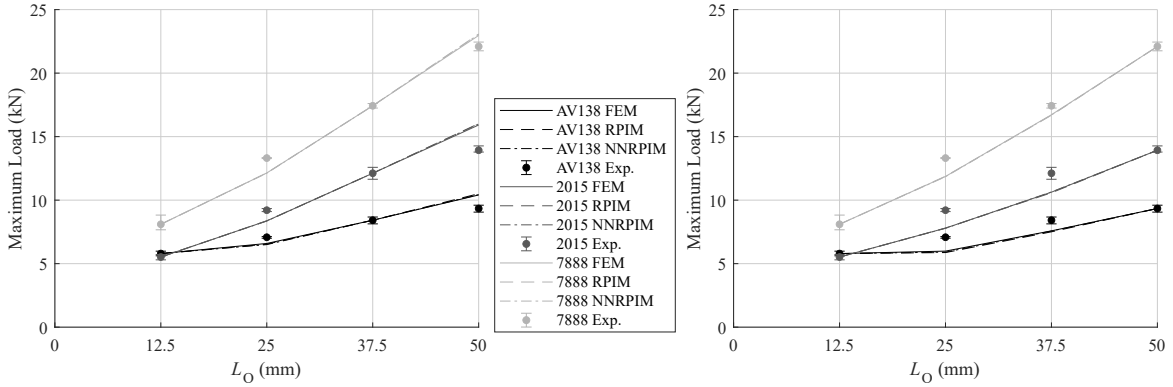

(a) (b)

Figure 5. Strength prediction using the parameters determined with (a) $L_{O1} = 12.5$ mm and $L_{O2} = 37.5$ mm (b) and $L_{O1} = 12.5$ mm and $L_{O2} = 50$ mm

the contrary, the lowest absolute error was 3.93%, 4.45%, and 4.32%, with the FEM, the RPIM and the NNRPIM, respectively. This occurred when predicting the strength of the joint with Araldite® 7888 and $L_O = 50$ mm. These predictions are shown in fig. 5a, from there it is possible to observe that the different numerical methods have minimal differences between them, which validates the use of the two meshless methods.

Considering that strength overpredictions are undesirable, a second L_O combination, where the predictions are always underpredictions, is also shown in fig. 5b. With this L_O combination the errors are slightly higher, with the highest error being 15.43%, 17.03%, and 16.56%, with the FEM, the RPIM and the NNRPIM, respectively. These errors are from the joint with Araldite® AV138 and $L_O = 25$ mm. While with this combination the lowest error was 4.04%, 4.27%, and 4.17%, with the FEM, the RPIM and the NNRPIM, respectively. These errors are from the joint with Sikaforce® 7888 and $L_O = 37.5$ mm.

4 Conclusions

This work made use of two different meshless methods, the RPIM and the NNRPIM, to predict the strength of SLJ using a continuum mechanics criterion, the CLS criterion. These strength predictions were accurate for all adhesives, which have significantly different properties. The comparison between the two meshless methods and the FEM also shows that the two meshless methods can be used to predict the strength of adhesive joints without any major drawbacks. The CLS parameters showed some variation depending on the L_O combination used to determine them. For these three adhesive it is advisable to use the shortest and longest L_O to determine them, but this could be different when using a different adherent.

Overall, this work shows that the RPIM and the NNRPIM are appropriate to be used in adhesive joints. However, the RPIM needs a restriction on the influence domains near the material interface, which is simple to implement. The strength predictions were accurate with the three different numerical methods.

Acknowledgements. The authors acknowledge the funding provided by Ministério da Ciência, Tecnologia e Ensino Superior – Fundação para a Ciência e a Tecnologia (Portugal), with the grants POCI-01-0145-FEDER-028351 and SFRH/BD/147628/2019. And the funding provided by LAETA with project UIDB/50022/2020.

Authorship statement. The authors hereby confirm that they are the sole liable persons responsible for the authorship of this work, and that all material that has been herein included as part of the present paper is either the property (and authorship) of the authors, or has the permission of the owners to be included here.

References

[1] O. Volkersen. Die Nietkraftverteilung in zugbeanspruchten Nietverbindungen mit konstanten Laschenquerschnitten. *Luftfahrtforschung*, vol. 15, pp. 41–47, 1938.
[2] C. C. De Sousa, R. Campilho, E. A. Marques, M. Costa, and L. F. Da Silva. Overview of different strength prediction techniques for single-lap bonded joints. *Proceedings of the Institution of Mechanical Engineers, Part L: Journal of Materials: Design and Applications*, vol. 231, n. 1-2, pp. 210–223, 2017.
[3] J. O. S. Silva, R. D. S. G. Campilho, and R. J. B. Rocha. Crack growth analysis of adhesively-bonded stepped joints in aluminium structures. *Journal of the Brazilian Society of Mechanical Sciences and Engineering*, vol. 40, n. 11, pp. 540, 2018.
[4] J. Belinha. *Meshless Methods in Biomechanics*. Springer, 2014.
[5] J. G. Wang and G. R. Liu. A point interpolation meshless method based on radial basis functions. *International Journal for Numerical Methods in Engineering*, vol. 54, n. 11, pp. 1623–1648, 2002a.
[6] L. M. Dinis, R. M. Natal Jorge, and J. Belinha. Analysis of 3D solids using the natural neighbour radial point interpolation method. *Computer Methods in Applied Mechanics and Engineering*, vol. 196, n. 13-16, pp. 2009–2028, 2007.
[7] L. D. Ramalho, J. M. Dionísio, I. J. Sánchez-Arce, R. D. Campilho, and J. Belinha. Analysis of stress singularity in adhesive joints using meshless methods. *Engineering Analysis with Boundary Elements*, vol. 137, n. July 2021, pp. 29–40, 2022.
[8] L. D. C. Ramalho, R. D. S. G. Campilho, and J. Belinha. Predicting single-lap joint strength using the natural neighbour radial point interpolation method. *Journal of the Brazilian Society of Mechanical Sciences and Engineering*, vol. 41, n. 9, pp. 362, 2019.
[9] L. D. Ramalho, R. D. Campilho, J. Belinha, and da L. F. Silva. Static strength prediction of adhesive joints: A review. *International Journal of Adhesion and Adhesives*, vol. 96, pp. 102451, 2020.
[10] G. Ji, Z. Ouyang, G. Li, S. Ibekwe, and S. S. Pang. Effects of adhesive thickness on global and local mode-I interfacial fracture of bonded joints. *International Journal of Solids and Structures*, vol. 47, n. 18-19, pp. 2445–2458, 2010.
[11] A. Y. Kanani, X. Hou, and J. Ye. The influence of notching and mixed-adhesives at the bonding area on the strength and stress distribution of dissimilar single-lap joints. *Composite Structures*, vol. 241, n. February, pp. 112136, 2020.
[12] da L. F. M. Silva and R. D. S. G. Campilho. *Advances in Numerical Modeling of Adhesive Joints*. Springer, 2012.
[13] M. R. Ayatollahi and A. Akhavan-Safar. Failure load prediction of single lap adhesive joints based on a new linear elastic criterion. *Theoretical and Applied Fracture Mechanics*, vol. 80, pp. 210–217, 2015.
[14] J. M. Dionísio, L. D. Ramalho, I. J. Sánchez-Arce, R. D. Campilho, and J. Belinha. Fracture mechanics approach to stress singularity in adhesive joints. *International Journal of Fracture*, vol. 232, n. 1, pp. 77–91, 2021.
[15] Q. Zhang, X. Cheng, Y. Cheng, W. Li, and R. Hu. Investigation of tensile behavior and influence factors of composite-to-metal 2D-scarf bonded joint. *Engineering Structures*, vol. 180, n. June 2018, pp. 284–294, 2019.
[16] O. C. Zienkiewicz and R. L. Taylor. *The Finite Element Method Volume 1 : The Basis*. Butterworth-Heinemann, 5 edition, 2000.
[17] L. W. Cordes and B. Moran. Treatment of material discontinuity in the Element-Free Galerkin method. *Computer Methods in Applied Mechanics and Engineering*, vol. 139, n. 1-4, pp. 75–89, 1996.
[18] J. Wang and G. Liu. On the optimal shape parameters of radial basis functions used for 2-D meshless methods. *Computer Methods in Applied Mechanics and Engineering*, vol. 191, n. 23-24, pp. 2611–2630, 2002b.
[19] D. Taylor. The theory of critical distances. *Engineering Fracture Mechanics*, vol. 75, n. 7, pp. 1696–1705, 2008.